Chopper-Modulated Locked in Amplified Gas Chromatography - Electroantennography Part II: Signal Processing and Performance Comparisons

Andrew J. Myrick and Thomas C. Baker

Abstract—A new method that improves gas-chromatography-electroantennographic detection through lock-in amplification is demonstrated. Here, measurements of antennal responses to major pheromone component, Z11-16:Ald, are performed under more optimal conditions, using saline electrical connections to excise antennae from male *H. subflexa*. Matched filtering in colored noise is applied to traditional enhanced graphics adapter recordings, allowing the signal to noise ratio of to be increased by about 6.1 dB (uncertainty is dependent on dosage). A dose-response model, including model parameter uncertainties is then used to estimate and compare performance in terms of naïve error rates involved in the detection of insect responses to GC peaks. Results indicate that relative performance is dosage dependent. Without a visible flame ionization detector (FID) reference peak for determining elution time, the model predicts the detection limit (placed at 5.0% expected naïve error rate) to be approximately 12 times lower using chopper modulation than when using traditional methods. At the highest traditional dosage tested, 10 pg, the equivalent chopper modulated dosage is estimated to be about 92 times lower. When a reference FID peak is clearly visible, the predicted detection limit (at 5.0% expected naïve error rate) is expected to be approximately 7 times lower using chopper modulation than when using traditional methods. At the traditional dosage of 10 pg, the predicted equivalent chopped dosage is estimated to be about 66 times lower.

Index Terms—Chopper stabilization, electroantennogram, GC-EAD, lock-in amplification, signal processing.

I. INTRODUCTION

PREVIOUSLY [1], the utility of lock-in amplification for the measurement of EAD signals was demonstrated. Relevant background of the GC-EAD technique is summarized there. Briefly, GC-EAD is a technique to identify volatile compounds that insects are sensitive to including pheromones and other ecological chemical signaling compounds which drive insect behavior. Here, under conditions that are more optimal for traditional measurements than in [1], we estimate the amplitude of EAD signal obtained from the male moth *H. subflexa* to its major pheromone component, using

excised antennae with low-noise saline connections to the EAD recording system. A simple "dose-response" model is then constructed to estimate detection error rates and the uncertainty in those estimates as a function of the amount of compound (pheromonal component) injected into the GC inlet.

The matched filter used in [1] is used to increase SNR and estimate signal amplitude. Matched filtering is also useful for signal detection. Briefly, detection theory involves deciding between two hypotheses given observations, generally noise alone or signal plus noise, using some boundary or threshold to separate the two classes. Errors include "misses" and "false alarms" in radar terminology. Here, naïve error rate, e, is minimized. $P_M(m)$ is used to refer to probability of missing a signal given the signal is present with the decision threshold at m. $P_{FA}(m)$ is the probability of deciding a signal is present given signal is not present with the detection threshold set at m. Naïve error rate is the detection error rate assuming no prior information is available about whether a signal is present or not resulting in the prior assumption of a 50% chance of signal being present. An error rate approaching 50% indicates that very little information can be obtained from the measurement. Using Bayesian methods, it is possible to form a statistical test utilizing a single threshold applied to the likelihood ratio to separate the two hypotheses given the observation(s) and some decision criteria [2]. For a known signal in Gaussian noise, the output of the matched filter is proportional to the log of the likelihood ratio and is optimal. Here, in the chopped case, the signal has an unknown amplitude and phase. Also, because the pheromone peak cannot be seen on the GC detector recording for the very low dosages used here, the location in time of the effluent peak is not known with certainty. Often, if signal parameters (such as amplitude) are not known, a general likelihood ratio test (GLRT) is used, which is proportional to the square of the magnitude of the matched filter output in Gaussian noise [3]–[5] (p. 244). Although the empirical noise probability density functions (PDFs) found here are not Gaussian, they have the desirable property that they are unimodal and monotonically decreasing. (Relevant methods for signal detection in non-Gaussian noise are dealt with in [6] but are not pursued here.) As a result, a likelihood ratio test (LRT) using a single threshold is still appropriate. Under chopped conditions, the magnitude of the matched filtered output and the squared magnitude are monotonically increasing functions of each

other, so a decision threshold may be chosen to satisfy decision criteria using either. However, under traditional conditions, signal magnitudes are assumed only to take on positive values. Under this condition, the likelihood ratio in Gaussian noise and the matched filter output (not squared) are also monotonically increasing functions of each other. Thus, a threshold can be chosen based on the matched filter output to satisfy decision criteria.

As discussed in [1], dose - response models have been constructed in the past. In [7], a linear regression was performed to relate the EAG voltages to pheromone component concentration on a log-log scale in both $T. ni.$ and $H. zea$. In [8], the rate of action potentials in single sensillum recordings (SSRs) was related to concentration through and empirical equation that at above noise levels is nearly linear on a log-log scale. Similarly, neural spike frequency and pheromonal component concentration in SSRs were related linearly on a log-log scale for the species $T. ni.$ in [9].

Our results also indicate that EAD signal and dosage may be linearly related on a log-log scale. Utilizing this simple relationship, we estimate distributions of parameters describing the linear model, and then estimate naïve error rate PDFs as a function of dosage using Monte Carlo methods. Using the error rate PDFs, we evaluated the ability of lock-in amplification to decrease the error rate. Two analyses were performed. The more simple comparison was made for situations when the timing of the EAG depolarization is known exactly, for instance when the GC detector peak is visible on the flame ionization detector (FID) and any timing skew between the GC detector and the EAD is known. This comparison will be referred to as a known timing (KT) comparison. The other analysis assumes the position of the peak is known within 5 seconds, which was the case in our measurements using pheromonal components not visible on the FID. This comparison will be referred to as an uncertain timing (UT) comparison. Relative performance was evaluated by comparing error rate PDF estimates obtained from dose-response models of both traditional and chopped techniques. The comparison was made by constructing PDFs of the ratio of traditional dosage to chopped dosage that achieve the same error rate through a range of given traditional dosages.

II. Methods

Dose-response measurements of both traditional and 8 Hz - chopped recordings were made to compare performance of the two techniques. The experimental setup for both chopped and traditional recordings was the same as that described in [1] (also see Fig. 3 in [1]). For both chopped and traditional preparations, several measurements were made at half-decade spaced dosages of $Z11$-16:Ald on male antennae of $H. subflexa$. Dosages are based on an assumed 1:2 split ratio between the FID and the EAD preparation; for each trial, two μL of each dosage was injected into the GC inlet. For chopped preparations, increasing dosages of $Z11$-16:Ald applied were 0.01, 0.033, 0.1, 0.33, 1.0, and 3.3 pg. On traditional preparations, dosages applied were 0.01, 0.033, 0.1, 0.33, 1, 3.3, and 10 pg.

Following this, signal demodulation (on chopped recordings) and matched filtering were applied to the waveforms

from which maximum likelihood estimates (MLE) of the normalized amplitudes were made. On traditional recordings without matched filtering, a simple peak search was used. To account for estimation uncertainty and bias in the non-Gaussian noise, empirical noise and signal plus noise models were constructed using Monte Carlo methods. The MLEs of normalized amplitudes were used to estimate 3-parameter PDFs for a dose-response model applied to three types of recordings: traditional, matched traditional, and matched chopped. Monte Carlo techniques were then used to estimate naïve error rate PDFs from the model parameter PDFs achieved using optimal thresholds in both KT and UT analyses for each recording type. Methods for comparison of the traditional recordings to chopped recordings are also described.

The number of traditional recordings was increased by including low-pass filtered versions of chopped recordings. Although it may be argued recordings were made using different odor delivery systems, both sets of data taken individually resulted in similar models, so we found it beneficial to the model to combine them, adding a low-SNR set of measurements taken at 0.01 pg to be used in the traditional model. These help to evaluate the form of the model. It should also be documented that some recordings were discarded for various reasons. Every recording made was considered and discarded for one of three reasons. The electrode holders tended to accumulate rust that found its way into the saline and had to be cleaned periodically. The presence of rust created recordings with significantly higher noise than encountered normally; recordings having large amounts of noise were discarded. If the noise segment contained unusual large excursions from the baseline it was discarded. Last, if the recording was incomplete or aborted for some reason, it was not used.

A. Gas - Chromatograph Settings

An Agilent 6190N GC was operated in splitless mode using a DB-5 type column, 30 m in length, 0.32 mm dia., with a 0.25 μm internal coating. The GC was operated in constant flow mode with a flow rate of 7.0 mL/min Helium carrier gas. The oven temperature was started at 100 degrees C, held for 1 minute and raised to 185 degrees C at 50 degrees C/min. The temperature was then raised from 185 degrees to 210 degrees at 10 degrees C/min. Following this, the temperature was raised to 300 degrees at 40 degrees C/min and then held for a 3 minute bakeout period. The inlet and FID detector were held at 310 degrees C.

B. Antennal Preparations

Recordings were made from either excised antennae electrically connected to by saline. Excised saline antennae with the first few terminal segments removed were connected through two borosilicate capillary tubes (World Precision Instruments, part number 1B150F-4) filled with saline. The capillary tubes were drawn to sharp tips which were scored and broken off so that the antenna would fit snugly inside for mechanical stability.
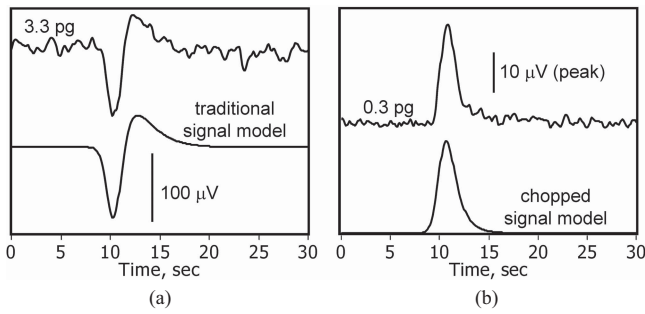
Fig. 1. Signal models decimated to 10 Sa/s. (a) Upper trace: traditional recording. Dosage is indicated. Lower trace: traditional signal model with MLE of the upper trace's amplitude applied. (b) Upper trace: estimated in-phase signal component of a demodulated chopped recording. Lower trace: chopped signal model with MLE of the upper trace's amplitude applied.

C. GC-EAD Recording System

The system used for making GC-EAD recordings was manufactured by Syntech (The Netherlands). This system uses a 10x preamplifier powered by the IDAC2 A/D converter. GC-EAD 2009 ver. 1.01, downloaded from sourceforge.com, was used to interface to the IDAC2. The selected range setting was "15.6 mV". Recordings were initiated by the start signal from the GC. Data were later exported in a text format and scaled to the appropriate voltage for post acquisition analysis using Labview from National Instruments.

D. Signal and Noise Models and Matched Filtering

Signal and noise models were constructed using the methods described in [1]. Signals were created in 20 second windows, from a Gaussian shaped pulse centered at 10 seconds. Fig. 1 is included for visualization of the signal models compared to recorded waveforms.

Parameters used for signal and noise modeling used the noise segment from 275 to 465 s to calculate the autocovariance, the Gaussian pulse input was modeled with a full width at half maximum (FWHM) value of 1.5 s, the peak tailing time constant was 1 s and the highpass time constant was 1.59 s.

E. Monte Carlo Estimation of Signal Plus Noise Distributions

As in [1], normalized amplitude estimates (measurements) are made by dividing MLE estimates of amplitude by the root mean square (RMS) power of matched-filtered noise alone, $\hat{\delta}_{vm}$

$$m = \hat{a}_N = \frac{|\hat{a}|}{\hat{\delta}_{vm}}. \qquad (1)$$

Although this method of estimating the normalized amplitude contains most of the information available, it suffers from bias and noise is non-Gaussian. To counter this, Monte Carlo methods were used to generate tabulated elements of empirical two dimensional conditional cumulative distribution functions (CDFs)

$$F_M\left(m_i \,|a_{N_j}\right) \qquad (2)$$

where m refers to the MLE of the normalized amplitude given by (1) and a_N is its deterministic value. Signal plus noise

distributions (2) were computed for both KT and UT analysis types. These were computed both to estimate model parameter PDFs from measurements (see section II. G.) and to generate signal plus noise distributions in Monte Carlo iterations used to estimate error rate and its uncertainty (see sections II H. 3 and II H. 4). Distributions (2) were computed from noise data pooled from all waveforms collected from each experiment. One reason for this was to extend the tails of the distributions so that error rates could be estimated over a larger dosage range. Expected measurement densities could also be assigned to one model rather than many separate models for display. Tabulated CDFs had resolution of 0.1 noise standard deviations for both a_N and m for all three recording types.

1) UT (Unknown Timing) Distributions: A matched signal template for each of each recording was generated by passing the signal model through its matched filter. Following this, 52 point (at 10 Sa/s) contiguous segments were drawn from a discrete uniform distribution covering every starting position in the waveform's noise segment. The matched signal of known size (a_N) was added to the noise segment with a centered and uniform positional uncertainty of 11 samples. Local maxima exceeding each measurement (m) threshold were counted after 180,000 iterations.

2) KT (Known Timing) Distributions: Empirical estimates of noise densities were made through summation of Gaussian Parzen windows with standard deviations given by Silverman's rule [10]. For traditional distributions, to generate each signal plus noise CDF, it was only necessary to translate the noise distribution by a_N. For chopped distributions, the signal plus noise PDFs were created by adding a_N to the baseband in-phase (I) noise segments, and then estimating the PDF of the resulting magnitude using Gaussian Parzen windows with standard deviations given by Silverman's rule [10].

F. Dose-Response Model

Estimates of naïve error rate PDFs are based on a simple 3-parameter model assuming a linear relationship between the log of the median of density of a_N and the log of the dosage injected into the GC. The log of the median of a_N is assumed to vary linearly with the log of the dosage. That is, linear and Gaussian distributed on a log-log scale

$$f_A\left(a_N \,|\mu, \sigma\right) = \frac{1}{a_N \sigma \sqrt{2\pi}} e^{-\frac{(\ln a_N - \mu)^2}{2\sigma^2}}. \qquad (3)$$

The equation describing the median is given by

$$\mu = k \ln d + b \qquad (4)$$

where k is the slope parameter, d is the dosage in pg and b is the y-axis intercept (1 pg dose). The model parameters (k,b,σ) will also be referred to as the parameter vector θ for the dose-response model.

SNR as a function of dosage was also modeled; SNR is simply equal to $|a_N|^2$. Thus it is also assumed log-normally distributed according to the following equation:

$$f_{SNR}\left(SNR \,|\mu, \sigma\right) = \frac{1}{SNR2\sigma \sqrt{2\pi}} e^{-\frac{(\ln SNR - 2\mu)^2}{2(2\sigma)^2}} \qquad (5)$$

where μ is given by (4). SNR is converted to decibels using the usual relation

$$SNR_{dB} = 10 \log_{10}(SNR).\qquad(6)$$

G. Generation of the Model Parameter PDF

Using tables for (2) in conjunction with measurements allows a model parameter PDF (used for for sampling in Monte Carlo iterations) to be obtained through Bayesian inference. Generation of the posterior density of the model parameters given K measurements (assuming uniform prior information, $f(\theta)$, here) is generated via Bayesian inference [11] based on the following equation:

$$f_\Theta(\theta \,|m_1 \ldots m_K, d_1 \ldots d_K) = \frac{f_\Theta(\theta) \prod\limits_{k=1}^{K} f_M(m_k|\theta, d_k)}{\int_{R^3} f_\Theta(\theta) \prod\limits_{k=1}^{K} f_M(m_k|\theta, d_k)d\theta}$$

$$= \frac{\prod\limits_{k=1}^{K} f_M(m_k|\theta, d_k)}{\int_{R^3} \prod\limits_{k=1}^{K} f_M(m_k|\theta, d_k)d\theta}\qquad(7)$$

where $f_M(m\,|\theta, d)$ can be described as the probability density of obtaining m given the model parameters and dosage associated with the measurement. This density can be obtained using the following equation:

$$f_M(m\,|\theta, d) = \int_{-\infty}^{\infty} f_A(a_N|\theta, d) f_M(m\,|a_N)da_N\qquad(8)$$

$f_A(a_N|\theta, d)$ is the log-normal model obtained by applying the model parameters k and b to (4) and substituting the result for μ into (3). It should be noted that $f_M(m\,|a_N)$ is entirely independent of θ and d. Values of the PDF, $f_M(m\,|a_N)$, used for computations at regular intervals of m are obtained from (2) via finite differences between adjacent tabulated CDF values

$$f_M(m_i\,|a_{N_j}) = [F_M(m_i\,|a_{N_j}) - F_M(m_{i-1}\,|a_{N_j})]/\Delta m\qquad(9)$$

where $\Delta m = 0.1$. Given some arbitrary measurement m_k, $f_M(m_k\,|a_{N_j})$ is estimated using linear interpolation between computed values of (9) associated with neighboring values of m. Riemann sums are used to approximate (8)

$$f_M(m_k\,|\theta, d_k) = \sum_{j=0}^{j_{max}} f_A(j\,\Delta a_N|\theta, d_k) f_M(m_k\,|a_{N_j}) \Delta a_N\qquad(10)$$

where $\Delta a_N = 0.1$. j_{max} corresponds to the maximum value of j for which $f_M(m_k\,|a_{N_j})$ is greater than 0.

Three (traditional, matched traditional, and matched chopped) 3-parameter distributions were constructed; PDFs of were computed from the measurements and stored in lookup tables with high resolution and negligible density outside their range ($100 \times 100 \times 100$ elements). The integral in the denominator of (7) was computed through Riemann sums over the domain of the lookup table.

H. Monte Carlo Simulations

Monte Carlo simulations drawing from tables of the dose-response model parameter distribution, (7), were used to estimate several quantities and PDFs. For illustration of the model, expected model parameter values, $E[\theta]$, dosage dependent measurement distributions based on the expected model parameters and dosage-dependent SNR and the distribution of its expected values were found. For the purpose of performance characterization and comparison, the PDF of the error rate as a function of dosage was based on thresholds that were optimized at each dosage. Optimal thresholds were determined by minimizing the expected error rate and then used in a second set of Monte Carlo simulations to estimate optimal error rate distributions as a function of dosage.

Sampling from the PDF of the model parameters, (7), during Monte Carlo simulations was accomplished using the conditional sampling method [12] (p. 555). Marginal and conditional marginal distributions were computed and stored in tables via Riemann sums of the density function values obtained from (7). Each marginal distribution was sampled using the inversion principle [12] (p. 27).

1) Expected Model Parameters: Expected values, $E[\theta]$, and standard errors of the model parameters were estimated from 10^4 samples drawn from each model parameter density.

2) Modeled Measurement Distributions: The expected values of θ were used to predict the expected value, 16th and 84th percentiles of measurements as a function of dosage based on the dose-response model. The expected value of measurements at a given dosage was obtained from the PDF, (10), in the usual manner using Riemann sums as an approximation to the integral

$$E[m\,|E[\theta], d_k] \cong \sum_{i=-30}^{i_{max}} m_i f_M(m_i\,|E[\theta], d_k)\Delta m\qquad(11)$$

where $m_i = i\,\Delta m$ and $\Delta m = 0.1$. (11) was evaluated at $d_k = 10^{(k/2-4)}$ pg for $k = \{0,1,\ldots,8\}$. i_{max} corresponded to the maximum value of i for which $f_M(m_i\,|E[\theta], d_k)$ was greater than 0. Densities obtained from (10) were numerically integrated using Riemann sums to obtain the corresponding CDF

$$F_M(m_i\,|E[\theta], d_k) = \sum_{l=-30}^{i} f_M(l\,\Delta s\,|E[\theta], d_k)\,\Delta s\qquad(12)$$

where $\Delta s = 0.1$. The CDF was used to find the 16th and 84th percentiles of the expected measurement distribution at each dosage.

3) Modeled SNR Distributions: The distribution of the expected value of the modeled SNR was estimated. The expected value of the SNR is given by

$$E[SNR|\mu, \sigma] = \exp\left(2\mu + (2\sigma)^2/2\right).\qquad(13)$$

10^4 samples of θ were drawn from the model parameter distribution and used to evaluate (13) using (4) at the same dosages enumerated for measurement distributions (section II H. 2). For viewing, the average value of the expected SNR was computed and the 16th and 84th percentiles of the expected SNR at each dosage were found by sorting the Monte Carlo results.

4) Error Rate Computations: Distributions of modeled error rates, $f_E(e|d_k, T_{Ok})$, were computed using thresholds chosen to minimize the expected error rate at each dosage where T_{Ok} refers to the optimal threshold at the kth dosage. These computations were made only for the two matched-filtered models, traditional and chopped (and not the unmatched traditional model). The optimal threshold was chosen so that the expected naïve error rate, $(P_{FA} + P_M)/2$, was minimized, requiring sampling of both the miss probability P_M and the false alarm probability, P_{FA}.

a) Sampling P_M: $P_M(T)$, where T is the threshold, includes uncertainty due to the measurement distribution, $f_A(a_N|\mu, \sigma)$ the model parameter distribution, $f_\Theta(\theta|m_1 \ldots m_K, d_1 \ldots d_K)$ and noise in the measurements. Its value is equal to the CDF corresponding to the PDF in (10). The nth sample, θ_n, drawn from the dose-response model parameter space is used to generate a corresponding signal plus noise density, $f_M(T_l|\theta_n, d_k)$ (see (10)), repeated here with subscripts for clarity

$$f_M(T|\theta_n, d_k) = \sum_{j=0}^{j_{\max}} f_A(j\Delta a_N|\theta_n, d_k) f_M(T|a_{N_j}) \Delta a_N$$

(14)

which is then converted to the CDF

$$F_M(T_i|\theta_n, d_k) = \sum_{l=-30}^{i} f_M(l\Delta s|\theta, d_k) \Delta s.$$ (15)

(14) was evaluated from $l = -30$ to 500 for each dose, d_k and parameter sample, θ_n. Calculations were carried out with $m_l = 0.1l$ and $\Delta a_N = 0.1$. (15) was then evaluated to obtain $P_{Mnk}(T_l)$. k ranged from 0 to 51 for traditional measurements and 0 to 35 for chopped measurements with $d_k = 10^{(0.1k-4)}$.

b) Sampling P_{FA}: $P_{FA}(m)$, which is equal to 1 - $F_M(m|a_N = 0)$ (see (2)), is obtained differently for simulations of threshold tests on UT and KT type analyses. For UT type analyses, the false alarm CDF was re-sampled with replacement (n out of n) [13]. It was found that series' of local maxima were uncorrelated and so they were assumed sufficiently independent for re-sampling. To generate the sample space, a 52 sample (5 second window of maxima) window was slid along each noise segment, storing the maximum value for each position of the window. Because local maxima appeared between 1 and 50 times, constituting 50 classes of data, the maxima were sorted into 50 classes, corresponding to how many times they appeared. Large local maxima were likely to appear 50 times in a row (likely to be the largest peak in a 10 second interval). The data in each class were re-sampled (n out of n) separately and smoothed using Gaussian Parzen windows with widths given by Silverman's rule [10]. The 50 PDFs were then weighted by the number of times they appeared and super-positioned to generate the re-sampled PDF.

For KT type simulations, all data in the noise segments were combined and smoothed using Gaussian Parzen windows with widths given by Silverman's rule [10]. The noise CDF was not resampled simply because we did not correct for the non IID (independent and identically distributed) EAD noise. Despite this, for both types of Monte Carlo simulations, the majority of

the uncertainty in error rate estimation was in the signal plus noise distributions (i.e. model parameter distribution) and not the noise distributions.

c) Detection threshold optimization: To optimize threshold, 10^3 Monte Carlo simulations were used to estimate expected error rates from the model parameter distribution through a range of dosages and thresholds, choosing and storing the threshold that minimized the expected error rate for each dosage. Near the minimum, resolution was increased to 0.01 noise standard deviations using spline interpolation to estimate both the error rate and the optimal threshold.

d) Error rate distributions: After optimal thresholds for each dosage were found, 10^4 Monte Carlo iterations were used to estimate optimized error rate densities, $f_E(e|d_k, T_{Ok})$. Expected values of error rates were obtained by averaging, while 16th and 84th percentiles were obtained by sorting the Monte Carlo error rates.

I. Performance Comparison

Performance comparison of two methods entailed finding the PDF of the ratio between the traditional dosage and chopped dosage given the same error rate and uniform positive prior densities for d_t and d_c

$$f_R\left(d_t d_c^{-1}|d_t\right)$$ (16)

where d_c refers to the chopped dosage and d_t refers to the traditional dosage. Because of the many orders of magnitude encountered in both error rate and dosage, numeric calculations are easier on a log-log scale where log-transformed variables are defined as

$$d_{lt} = \ln(d_t)$$
$$d_{lc} = \ln(d_c)$$
$$e_l = e_{lt} = e_{lc} = \ln(e).$$

Error rate PDFs, $f_E(e|d_k)$ (note the optimized threshold is assumed and left out from here forward), as functions of dosage used for performance comparisons were obtained by superpositioning Gaussian Parzen windows with widths that were half of that given by Silverman's rule [10]. Estimated densities of error rate were log transformed using the following equation, where tables of $f_E()$ had already been stored on a log scale of dosage:

$$f_{El}(e_l|d_l) = \exp(e_l) f_E(\exp(e_l)|d_l).$$ (17)

The expected value of the ratio d_t/d_c can be obtained from the following equation:

$$E\left(d_t d_c^{-1}|d_t\right) = d_t \int_0^\infty d_c^{-1} f_{Dc}(d_c|d_t) dd_c$$
$$= \exp(d_{tl}) \int_{-\infty}^\infty \exp(-d_{cl}) f_{Dcl}(d_{cl}|d_{tl}) dd_{cl}.$$

(18)

Percentiles may be obtained from the CDF

$$F_R\left(d_t d_c^{-1}|d_t\right) = \int_{-\infty}^{\ln(d_t d_c^{-1})} f_{Dcl}(d_{tl} - x_{cl}|d_{tl}) dx_{cl} = P.$$ (19)

Thus an expression for $f_{Dcl}(d_{cl}|d_{tl})$ is desired for substitution into (18) and (19). No additional information about d_{cl} can be obtained from d_{tl} when the error rate is known. Thus

$$f_{Dcl}(d_{cl}|e_{cl},d_{tl}) = f_{Dcl}(d_{cl}|e_{cl}). \qquad (20)$$

Setting $e_t = e_c = e$

$$f_{Etl}(e_{tl}|d_{tl}) f_{Dcl}(d_{cl}|e_{cl}=e_{tl}) = f_{El,Dcl}(e_l,d_{cl}|d_{tl}). \qquad (21)$$

$f_{Dcl}(d_{cl}|d_{tl})$ is obtained by integrating out the error rate from the PDF in (21)

$$f_{Dl}(d_{cl}|d_{tl}) = \int_{-\infty}^{\infty} f_{Etl}(e_l|d_{tl}) f_{Dcl}(d_{cl}|e_l) de_l. \qquad (22)$$

However, an expression for $f_{Dcl}(d_{cl}|e_l)$ is necessary for the evaluation of (22). Through Bayesian inference

$$f_{Dcl}(d_{cl}|e_l) = \frac{f(d_{cl}) f_{Ecl}(e_l|d_{cl})}{\int_{-\infty}^{\infty} f(d_{cl}) f_{Ecl}(e_l|d_{cl}) dd_{cl}}. \qquad (23)$$

The uniform (linear-scale, positive) prior density, $f_D(d_c)$, can be log-transformed using the following equation:

$$f_{Dl}(d_{cl}) = \exp(d_{cl}) f_D(\exp(d_{cl})). \qquad (24)$$

Substituting (24) into (23) results in the following expression:

$$f_{Dcl}(d_{cl}|e_l) = \frac{\exp(d_{cl}) f_{Ecl}(e_l|d_{cl})}{\int_{-\infty}^{\infty} \exp(d_{cl}) f_{Ecl}(e_l|d_{cl}) dd_{cl}}. \qquad (25)$$

Finally, substitution of (25) into (22) results in an expression for $f_{Dcl}(d_{cl}|d_{tl})$ that is desired for substitution into (18) and (19). At traditional dosages above which full densities given by (22) could not be calculated, the ratio $d_t d_c^{-1}$ is shown under the condition

$$E(e_t|d_t) = E(e_c|d_c). \qquad (26)$$

III. RESULTS

Results include plots of typical EAD recordings, modeled SNR and measurement distributions as a function of dosage, modeled error rates as a function of dosage and our relative performance measure, estimated equivalent dosage ratios as a function of traditional dosage. Tabulated results include dose response model parameters, measurements and model predictions.

Fig. 2 shows typical recordings at each dosage, selected because the normalized amplitude of each was near the mean at that dosage. Panel A shows raw traditional waveforms recorded under the conditions described in the methods. Panel B shows the same recordings with matched filtering applied, scaled to estimate amplitude the Gaussian pulse input [1]. Panel C shows the (estimated) in-phase component of demodulated chopped recordings with the carrier magnitude just before the signal occurrence subtracted out. Demodulated chopped recordings have the advantage that less noise is present at low frequencies. Thus, shapes of peaks with low frequency content, such as the hexane solvent peak can be seen. Distortion is introduced by matched filtering of chopped waveforms (i.e. panel D), though SNR does exhibit an increase.

Traditional recordings have a tendency to have large deviations from the baseline such as that present on the 3.3 pg trace (Panel A) which are eliminated by chopping. For instance, the demodulated 3.3 pg waveform is not visually differentiable from noise where the large deviation is seen on the traditional waveform (not shown).

The expected values and standard error of the dose-response model parameters are shown in Fig. 3. Based on the values of intercept, b, an estimate of the SNR improvement to traditional waveforms by matched filtering is 6.0 ± 0.6 dB. The slope of the SNR in matched traditional recordings is 6.0 ± 0.3 dB per decade of dosage. This result is similar to that found in (Mayer et al. 1987), where 1 to 2 second Z11-16:Ald pulses delivered to male *H. zea*, antennae (similar to *H. subflexa*) resulted in a slope of 7.3 dB per decade of concentration. On the other hand, chopped EAD SNR was found to increase at a rate of 8.4 ± 0.5 dB per decade of dosage. Dose-response model fits to demodulated responses at harmonics of 8 Hz (not shown here) resulted in slopes that increased with frequency, up to 24 Hz, where at 32 Hz, only the 3.3 pg responses were above noise. Based on this observation, it seems likely that the "frequency responses" of antennae are a function of concentration, responding slower at lower concentrations.

Table 1 summarizes experimental results and selected results from Monte Carlo simulations. N refers to the number of EAD measurements at each dosage, P_M is the estimated probability of a miss, and M is the actual miss count out of the N trials. The mean normalized amplitude for traditional unmatched estimates coincide well with the dose response model, except at 10 pg. Similarly for traditional matched estimates of normalized amplitude, the measurements and the model coincide well, except at 0.1 pg. Last, the chopped model had two dosages that did not coincide well with measurements at 0.1 and 0.33 pg. It should be noted here also that chopped responses did not follow the linear (log-log) model above 3.3 pg to 10 pg, where the EAD responses exhibited saturation and did not increase as a result of the increase in dosage. The empirical noise density did not extend far enough to estimate error rates above dosages of 0.25 pg in the chopped model. Miss counts are very reasonable for all the models, given the predicted P_M. However, this is not the case when thresholds are employed at other levels, (not shown) reflecting a mismatch between the assumed log-normal density and the actual densities encountered, complicated by uncontrolled experimental factors. Some of these include the variation in the age of the moths used, the varying time required to prepare an antenna, and some differences due to the two measurement methods used for traditional data. Other factors difficult to control are the spatial configurations of the antennae, each of which orients its sensilla and twist and bend in unique ways in response to the mechanical chopping. The exact coverage of the antenna by saline at its ends is also difficult to control.

Fig. 3(a) shows the modeled expected SNR as a function of dosage and its 16th and 84th percentiles for each type of measurement employed. The difference in slope between chopped and traditional measurements is apparent, as is the 6 dB improvement in SNR achieved by the matched filtering on traditional waveforms. It can also be seen that the uncertainty at extrapolated dosages is higher. In panels B, C, and D, the dose response model corresponding to the expected values of
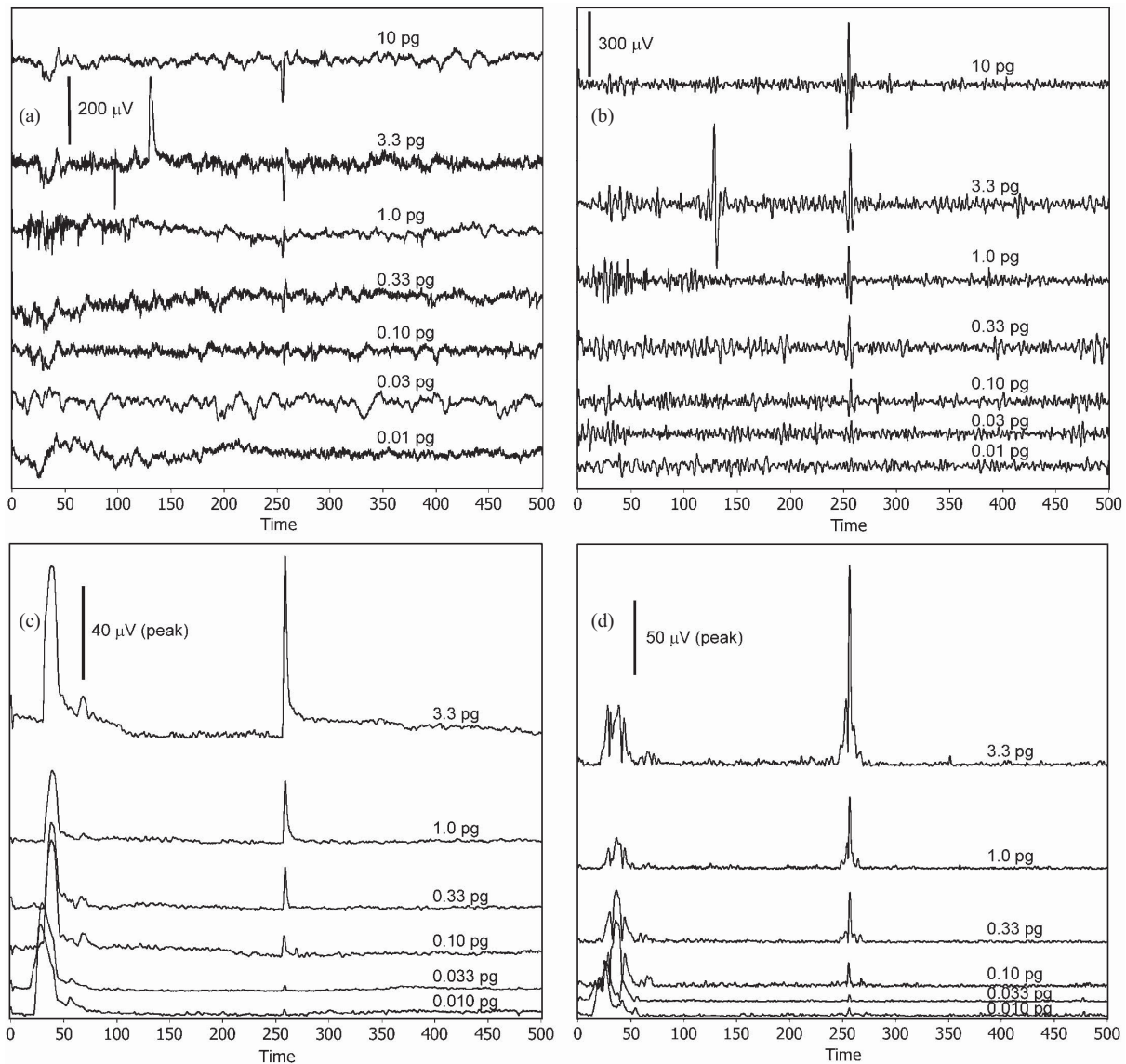
Fig. 2. Dose-response EAD recordings. Z11-16:Ald odorant elutes at 257 s. Vertical scale and dosages are labeled. (a) Traditional. (b) Traditional after matched filtering. (c) Chopped and demodulated. (d) In-phase component.

TABLE I
UT DOSE-RESPONSE MONTE CARLO RESULTS

| Dose, pg | N | Traditional unmatched | | | | | Traditional matched | | | | N | Chopped matched | | | M |
		Mean $a_N \pm$ SE	Model E[a_N]	$P_M \times 10^2$	M		Mean $a_N \pm$ SE	Model E[a_N]	$P_M \times 10^2$	M		Mean $a_N \pm$ SE	Model E[a_N]	$P_M \times 10^2$	M
0.01	16	2.18±0.34	2.22±0.15	34±4	7		3.45±0.52	3.50±0.25	23±4	5	18	6.11±0.52	6.48±0.88	5.0±2.0	1
0.033	23	3.30±0.47	2.81±0.18	28±4	7		4.93±0.45	4.78±0.29	13±3	3	13	9.38±0.72	10.1±0.7	1.0±0.1	0
0.10	15	3.54±0.48	3.69±0.20	20±3	3		5.43±0.57	6.64±0.33	4.5±2.1	1	9	13.10±1.84	16.8±1.0	0.48±0.054	0
0.33	14	5.02±0.64	4.97±0.23	13±2	3		10.3±1.1	9.30±0.41	3.1±1.0	0	7	36.0±3.5	28.1±1.8	N/A	0
1.0	18	7.29±1.02	6.80±0.32	6.4±2	1		14.5±1.1	13.1±0.6	1.0±0.5	0	12	46.6±5.4	47.1±4.0	N/A	0
3.3	13	7.98±1.42	9.41±0.55	2.8±1	1		19.4±3.7	18.4±1.0	0.30±0.20	0	8	73.8±9.8	79.1±8.7	N/A	0
10	23	15.2±1.2	13.1±1.0	1.0±0.5	0		23.7±1.6	25.7±1.7	0.13±0.10	0					

the parameters included on the upper right corner of each panel was used to compute the expected value of the measurements and their 16th and 84th percentiles as a function of dosage for the three measurement types. As dosage is lowered, it is evident the modeled measurements asymptotically approach the noise floor in all three panels. Points corresponding to the actual measurements are superimposed, where outliers and deviations from the model are apparent in the data.

Modeled error rates (expected value, 16th and 84th percentiles) as a function of dosage are plotted in Fig. 4(a)
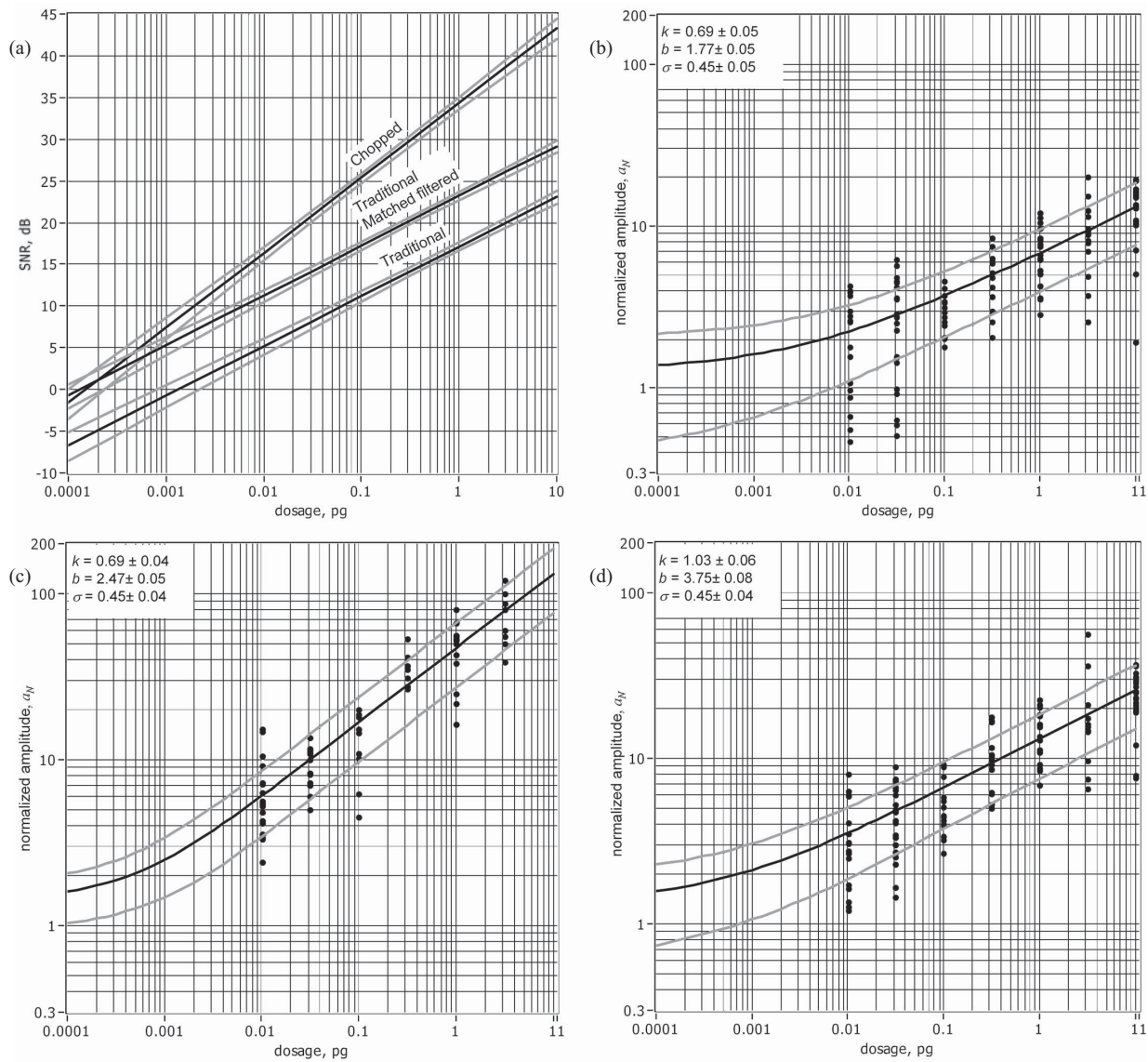
Fig. 3. (a) Expected SNR [see (13)] for all three models including their 16th and 84th percentiles. (b)–(d) Expected value, 16th and 84th percentiles of expected models, $f_M(m|E[\theta], d_k)$ [see (10)] with measurements superimposed. Model parameters and their standard deviations are indicated in the upper left corner of each panel. (b) Traditional model and normalized amplitude measurements. (c) Traditional matched filtered model and normalized amplitude measurements. (d) Chopped model and matched filtered normalized amplitude measurements.

and Fig. 4(b), where they can be compared visually. Error rates are seen to be much lower for chopped measurements at higher dosages, but the improvement decreases with decreasing dosage. In Panel A, the expected error rates intersect at about 2×10^{-4} pg, where the error rate is expected to be very high and unlikely to be useful. Considering Panel B, it is evident that knowing the elution time of the peak significantly reduces the error rate for both chopped and traditional methods, but even more so for traditional methods.

The expected error rates intersect at about 5.5×10^{-5} pg at a potentially useful predicted error rate.

Fig. 5 summarizes the results of performance comparisons in terms of error rate as described in the methods. Panel A compares performance between chopped and traditional matched filtered methods for UT segments while Panel B displays the same comparison when elution times are known. The black line decreasing with dosage is the expected error
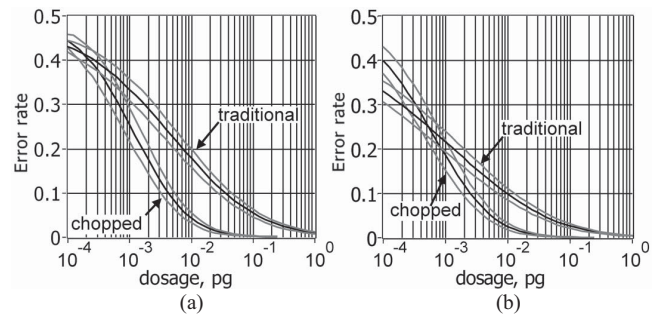

Fig. 4. Modeled error rates at optimized thresholds as a function of dosage including 16th and 84th percentiles. (a) Unknown timing (UT). (b) Known elution times (KT).

rate at the traditional dosage, whose scale is indicated on the left vertical axis. The expected dosage ratio from (17)
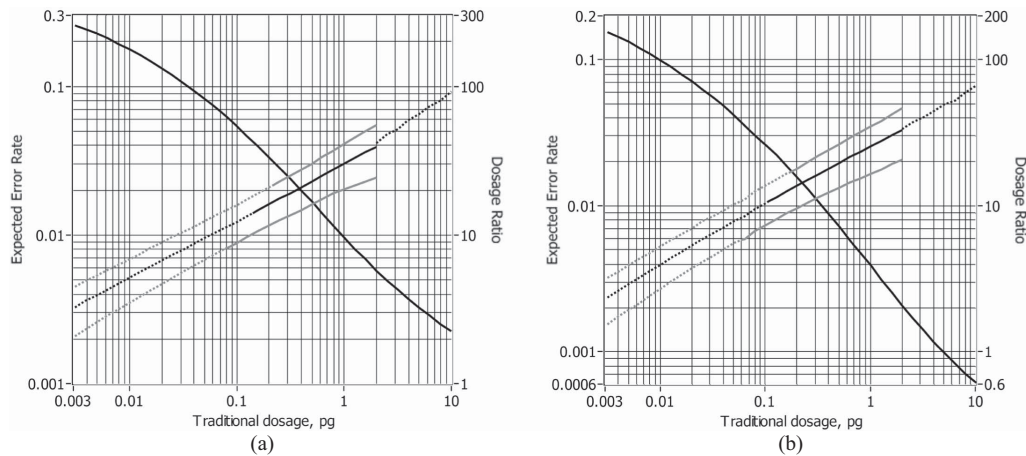
Fig. 5. Chopped equivalent dosage ratio and expected error rate versus traditional dosage. 16th and 84th percentiles are indicated for dosage ratios. (a) UT. (b) KT.

and 16th and 84th percentiles of its PDF computed from (18) are increasing functions of dosage, whose scale is given on the right vertical axis. The dotted portion at lower dosages indicates the dosage range which has been extrapolated lower than the dosages actually tested and is based on the dose-response model alone. Above 2 pg, the dotted line indicates the dosage ratio obtained under the condition given by (25).

For UT comparisons, the model predicted the detection limit (5.0% expected naïve error rate) to be 0.09 to 0.15 pg using traditional methods, compared to 0.007 to 0.012 pg using lock-in amplification. For comparison to the model, near the detection limit, the empirical probability of false alarm (P_{FA}) at a dosage of 0.1 pg using traditional methods was 3.6% while the number of missed EAD responses was 1/15 (6.7%) at the modeled optimal threshold. Similarly, using chopping at 0.01 pg, the empirical probability of false alarm was 3.4% while the number of missed EAD responses was 1/18 (5.6%) at the modeled optimal threshold. The highest traditional dosage for which equivalent chopped dosage estimates with uncertainty could be calculated was 2 pg, where equivalent chopped dosage was estimated to be 24 to 55 times lower. At the highest traditional dosage tested, 10 pg, the equivalent chopped dosage was estimated to be about 92 times lower (0.11 pg) based on error rate expectations.

For KT comparisons, the predicted the detection limit (5.0% expected naïve error rate) was expected to be 0.028 to 0.050 pg using traditional methods, compared to 0.0042 to 0.0072 pg using lock-in amplification. At 2 pg, equivalent chopped dosage was estimated to be 20 to 33 times lower than traditional dosage. At the traditional dosage of 10 pg, the predicted equivalent dosage ratio was 66, corresponding to a chopped dosage of 0.15 pg.

IV. Conclusion

We have evaluated two techniques, matched filtering and lock-in amplification, for increasing the performance of the GC-EAD instrument. Matched filtering in colored noise was used for linear filtering of the waveforms and is closely related to commonly used LRTs used for presence-absence decision making. A simple dose-response model was fitted

to collected data and estimates of optimal naïve error rate densities were made and compared. Although performance in terms of optimal error rates was compared, under most investigative conditions, when antennal response has not been modeled, a false alarm rate might be specified instead, resulting in different different threshold criteria. It should be noted here that preliminary results indicate similar performance advantages are predicted under a 5% expected false alarm rate criterion. Also, under investigative conditions, multiple trials would likely be used to determine presence of a signal at some time or times. This well known problem is known as sequential detection, and could be easily applied to EAD recordings.

Improvements to the chopping method are likely to be possible if the mechanical motion near the antennal preparation can be eliminated to reduce noise. In matched filtered chopped recordings, the noise level is about 3.5 dB higher than that found in EADs recorded under traditional conditions. From our model, an improvement in SNR of 3.5 dB is predicted to increase the dosage ratio by approximately a factor of two to three across all dosages. Increasing the efficiency of transfer of effluent to antennae is also another area that could be improved. The time course of the effluent peaks might also prove to be a useful variable.

Observations of the data also indicated that these antennae respond slower to lower concentrations of pheromone, suggesting that frequency content of modulated effluent could be optimized for different criteria while combining information available from the traditional signal, fundamental chop frequency or frequency band and its harmonics.

References

[1] A. J. Myrick and T. C. Baker, "Chopper stabilized gas chromatography-electroantennography part I: Background, signal processing and example," *Biosensors Bioelectron.*, vol. 31, no. 1, pp. 197–204, Jan. 2011.
[2] M. D. Srinath and P. K. Rajasekaran, *An Introduction to Statistical Signal Processing with Applications*. New York: Wiley, 1979, pp. 1–450.
[3] E. J. Kelly, I. S. Reed, and W. L. Root, "The detection of radar echoes in noise," *J. Soc. Ind. Appl. Math.*, vol. 8, no. 2, pp. 309–341, Jun. 1960.
[4] F. C. Robey, D. R. Fuhrmann, E. J. Kelly, and R. Nitzberg, "A CFAR adaptive matched filter detector," *IEEE Trans. Aerosp. Electron. Syst.*, vol. 28, no. 1, pp. 208–216, Jan. 1992.

[5] C. W. Helstrom, *Statistical Theory of Signal Detection*, vol. 9. New York: Pergamon Press, 1960.

[6] S. A. Kassam, *Signal Detection in Non-Gaussian Noise*. New York: Springer-Verlag, 1988.

[7] M. S. Mayer, R. W. Mankin, and A. J. Grant, "Quantitative comparison of behavioral and neurophysiological responses of insects to odorants: Inferences about central nervous system processes," *J. Chem. Ecol.*, vol. 13, no. 3, pp. 509–531, 1987.

[8] R. W. Mankin and M. S. Mayer, "Stimulus-response relationships of insect olfaction: Correlations among neurophysiological and behavioral measures of response," *J. Theoret. Biol.*, vol. 100, no. 4, pp. 613–630, Feb. 1983.

[9] R. W. Mankin, M. S. Mayer, and A. J. Grant, "Sensitivity of Trichoplusia ni (Hübner) pheromone receptor neurons: Relationships between neural thresholds and behavioral responses," *J. Comparat. Phys. A*, vol. 168, no. 6, pp. 739–747, 1991.

[10] B. W. Silverman, *Density Estimation*. London, U.K.: Chapman & Hall, 1986.

[11] V. Barnett, *Comparative Statistical Inference*, 2nd ed. New York: Wiley, 1982.

[12] L. Devroye, *Non-Uniform Random Variate Generation*. New York: Springer-Verlag, 1986.

[13] M. R. Chernick, *Bootstrap Methods: A Guide for Practitioners and Researchers*, 2nd ed. Hoboken, NJ: Wiley, 2008.

Andrew J. Myrick was born in Evanston, IL, in 1973. He received the B.S.E.E. degree from Bucknell University, Lewisburg, PA, in 1995, and the M.S. and Ph.D. degrees in bioengineering from the University of Illinois at Chicago, Chicago, in 2001 and 2005, respectively.

He was with Automatic Test Systems Division, Northrop Grumman Corporation, from 1995 to 1999. He is currently a Post-Doctoral Fellow with the Department of Entomology, Penn State University, University Park. His current research interests include signal processing, pattern recognition, and fluid mechanics.

Thomas C. Baker was born in Cleveland, OH, in 1950. He received the B.S. and M.S. degrees from Cornell University, Ithaca, NY, in 1972 and 1975, respectively, and the Ph.D. degree from Michigan State University, East Lansing, in 1979, all in entomology.

He was a Faculty Member with the Department of Entomology, University of California, Riverside, from 1979 to 1992, and Iowa State University, Ames, from 1992 to 2003. Since 2003, he has been a member of the Department of Entomology, Center for Chemical Ecology, Huck Institutes of the Life Sciences, Penn State University, University Park.